Published in final edited form as:
Ultrasound Med Biol. 2012 May ; 38(5): 753–766. doi:10.1016/j.ultrasmedbio.2012.01.013.

AN EFFICIENT TREATMENT STRATEGY FOR HISTOTRIPSY BY REMOVING CAVITATION MEMORY

Tzu-Yin Wang[*], **Zhen Xu**[*], **Timothy L. Hall**[*], **J. Brian Fowlkes**[*,†], and **Charles A. Cain**[*]
[*]Department of Biomedical Engineering, University of Michigan, Ann Arbor, MI, USA
[†]Department of Radiology, University of Michigan, Ann Arbor, MI, USA

Abstract

Cavitation memory effects occur when remnants of cavitation bubbles (nuclei) persist in the host medium and act as seeds for subsequent events. In pulsed cavitational ultrasound therapy, or histotripsy, this effect may cause cavitation to repeatedly occur at these seeded locations within a target volume, producing inhomogeneous tissue fractionation or requiring an excess number of pulses to completely homogenize the target volume. We hypothesized that by removing the cavitation memory, *i.e.*, the persistent nuclei, the cavitation bubbles could be induced at random locations in response to each pulse; therefore, complete disruption of a tissue volume may be achieved with fewer pulses. To test the hypothesis, the cavitation memory was passively removed by increasing the intervals between successive pulses, Δt, from 2, 10, 20, 50 and 100, to 200 ms. Histotripsy treatments were performed in red blood cell tissue phantoms and *ex vivo* livers using 1-MHz ultrasound pulses of 10 cycles at P–/P+ pressure of 21/59 MPa. The phantom study allowed for direct visualization of the cavitation patterns and the lesion development process in real time using high-speed photography; the *ex vivo* tissue study provided validation of the memory effect in real tissues. Results of the phantom study showed an exponential decrease in the correlation coefficient between cavitation patterns in successive pulses from 0.5 ± 0.1 to 0.1 ± 0.1 as Δt increased from 2–200 ms; correspondingly, the lesion was completely fractionated with significantly fewer pulses for longer Δts. In the tissue study, given the same number of therapy pulses, complete and homogeneous tissue fractionation with well-defined lesion boundaries was achieved only for $\Delta t \geq 100$ ms. These results indicated that the removal of the cavitation memory resulted in more efficient treatments and homogeneous lesions.

Keywords

Histotripsy; Cavitation memory; Efficient treatments; Homogeneous lesions

INTRODUCTION

Acoustic cavitation induced by high-intensity (peak negative pressure >10 MPa), extremely short (<50 μs) ultrasound pulses at low duty cycles (<1%) has been shown to mechanically fractionate soft tissue in a well-controlled manner (Xu et al. 2004; Parsons et al. 2006a; Roberts et al. 2006; Kieran et al. 2007). This process results in soft tissue ("histo-") disruption ("-tripsy"), which has given rise to the term *histotripsy*. Histotripsy has been actively investigated as a tool for noninvasive tissue ablation. Recent studies demonstrated promising results that histotripsy can noninvasively and precisely produce lesions in the

Address correspondence to: Tzu-Yin Wang, 2200 Bonisteel Blvd., Carl A Gerstacker Building, Ann Arbor, MI 48109. tzuyin@umich.edu.

target regions in many *in vivo* models (Kim et al. 2011; Maxwell et al. 2010a; Owens et al. 2010; Styn et al. 2010; Xu et al. 2010).

For cavitation-based therapy like histotripsy, the initiation and maintenance of the cavitation process is highly affected by the small gas bubbles in a host medium that serve as nuclei for cavitation (Leighton 1997). These nuclei may preexist in the host medium as gas pockets adhering to crevices on particles or stabilized with organic skin ("stabilized" nuclei), or they may form as fragments of bubbles that persist from collapse of transient cavities ("unstabilized" nuclei) (Harvey et al. 1944a, 1944b; Fox and Herzfeld 1954; Flynn and Church 1984). The unstabilized nuclei may become new cavitation sites that sustain subsequent cavitation events. This phenomenon, which has been discussed in the literature (Flynn and Church 1984; Henglein and Gutierrez 1986; Fowlkes and Crum 1988; Yavas et al. 1994), is referred as the *cavitation memory effect*.

The cavitation memory effect may be advantageous for cavitation-based therapies when the acoustic pressure is insufficient to consistently produce cavitation with each single pulse. In this case, the existence of the cavitation memory, or the persistent nuclei, may help sustain or enhance the cavitation process (Delius and Brendel 1988; Huber et al. 1999; Arora et al. 2005). This concept has been applied to improve the stone fragmentation efficiency in lithotripsy (Xi and Zhong 2000; Loske et al. 2002), or to enhance the tissue fractionation in histotripsy (Xu et al. 2005, 2006; Parsons et al. 2006a).

Despite the advantage of sustaining the cavitation process, the cavitation memory could be disadvantageous in some cases. One example is the energy shielding effect. In lithotripsy, the presence of the cavitation memory at a high pulsing rate (>2 Hz) can induce denser and longer persisting bubble clouds (Huber et al. 1998; Sapozhnikov et al. 2002). The growth of the persistent bubbles can detract energy from the shock waves and shield the energy delivery to the stone surface (Pishchalnikov et al. 2006), resulting in inefficient stone fragmentation (Weir et al. 2000; Paterson et al. 2002; Madbouly et al. 2005; Yilmaz et al. 2005). The excess bubbles can also cause more renal damage (Delius and Brendel 1988; Delius et al. 1988; Ryan et al. 1991). In histotripsy, similar pressure levels are used to generate cavitation for tissue fractionation. Concerns about the shielding effect may thus be raised. It is worth noting that although the pressure levels are similar, the waveforms are significantly different. Lithotripsy uses one acoustic cycle pulse with a long rarefactional phase, which provides ample time for bubble expansion and often generates large bubbles ~1 mm in diameter with a pulsing rate of 0.5–5 Hz (Huber et al. 1998; Sapozhnikov et al. 2002). Histotripsy uses pulse duration of a few acoustic cycles with much shorter rarefactional phase. The maximal bubble diameter is much smaller (~100 μm) in the regime that histotripsy commonly operates (PRF = 5 Hz to 1 kHz) (Xu et al. 2008; Maxwell et al. 2011). The energetic expansion and collapse of these smaller bubbles cause controlled fractionation of soft tissue. The shielding effect has been observed in histotripsy only when applied at a tissue-fluid interface with an extremely high pulsing rate (>10 kHz) (Xu et al. 2004, 2007a). This effect is insignificant in treatments applied within a volume of soft tissue with a common pulsing rate (5 Hz to 1 kHz).

For histotripsy treatments applied within a volume of soft tissue, the cavitation memory may cause a different undesired phenomenon. With the residual cavitation seeds present, the bubbles may be generated at the same seeded locations by the subsequent pulses. If the spatial distribution of the bubbles is not sufficiently dense, the areas where the cavitation bubbles repeatedly occur are overtreated, whereas the rest remain undertreated. This can result in inhomogeneous tissue disruption even within a single focal volume, producing islands of structurally intact tissues in the treatment volume when a small number of pulses is applied (Roberts et al. 2006; Wang et al. 2009). These islands of intact tissues could be

detrimental for applications where complete tissue removal is desired (*e.g.*, tumor therapy). In addition, when quantitative tissue characterization methods (*e.g.*, ultrasound spectrum analysis (Lizzi et al. 1997)) are used to assess the treatment outcomes, a misleading metric may be produced as an average of fully homogenized and nonhomogenized zones.

To completely and homogeneously fractionate the target volume, strategies to break the memory-induced repeated cavitation pattern are needed. One strategy is to deliver an excess number of pulses to the target volume until the cavitation bubbles migrate (sometimes slowly) to different locations in the target volume. However, this may cause inefficient use of energy and prolonged treatment time. Here we propose a strategy to achieve complete and homogeneous tissue fractionation with a significantly reduced number of pulses by removing the cavitation memory. The removal of the memory should cause cavitation bubbles to occur at random locations in response to each pulse. As long as the pressure amplitude is high enough so that the cavitation can be consistently induced in each pulse, this random pattern would allow the target volume to be homogeneously fractionated with fewer pulses.

This study investigates the cavitation pattern, *i.e.*, spatial distribution of the cavitation bubbles, in response to each histotripsy pulse and the corresponding lesion development process for different levels of cavitation memory. It is hypothesized that the cavitation memory would decrease with time as the persistent bubbles diffuse, dissolve and redistribute to new random locations. As such, the level of the persistent memory can be manipulated (passively) by increasing the time interval between successive pulses. Experiments were performed both in the red blood cell (RBC) tissue phantoms (Maxwell et al. 2010b) and in *ex vivo* liver tissues. The former allowed for direct visualization of the locations of the cavitation bubbles and the corresponding lesion development process in real time using high-speed photography; the latter provided validation of the memory effect in real tissues with histologic examinations. This study illustrates a significant effect of cavitation memory on the treatment progression, providing the basis for future design of efficient treatments.

METHODS

Sample preparation

The protocols described in this study were approved by the University of Michigan's Committee on Use and Care of Animals. An agarose-based RBC tissue phantom that allows for direct visualization of cavitation and the resulting damage was used to study the impact of the cavitation patterns on the lesion development process. The phantom was prepared with 1% agarose powder (Type-VII, Sigma-Aldrich, St. Louis, MO) and 5% v/v RBCs (from healthy adult research canines in an unrelated study) mixed in normal saline following the protocol described in our previous paper (Maxwell et al. 2010b). The phantom was constructed such that a thin (~0.5 mm) RBC-gel layer was suspended between two thick (~2.5 cm) transparent gel layers. The RBC-gel layer becomes transparent in the locations where the RBCs are damaged by cavitation, likely because the cell content (hemoglobin) is released. The transparent damaged regions are visible within a few milliseconds and become fully developed within 1 s. This period is likely the time required for sufficient hemoglobin to be released to the medium so that the light can penetrate through the damaged locations. The cavitation bubbles induced in the RBC phantom can be easily detected because they block the light transmission and appear as dark shadows on backlit optical images. During the treatment, both the cavitation bubbles and the lesion can be imaged with high-speed photography. Information regarding the size, shape and location of the bubbles and the lesion can be extracted with image processing algorithms described later in this section (*Cavitation pattern analysis and lesion analysis*).

To validate the cavitation memory effect on treatments in real tissues, experiments were also performed in freshly excised canine livers. The livers were obtained from healthy adult research subjects in an unrelated study post-euthanization. The excised tissues were placed in degassed (20 to 30% gas saturation) saline at room temperature and used within 3 hours of harvest. The tissues were sectioned into approximately 9 × 9 × 6-cm blocks and sealed in plastic bags filled with saline before experimentation.

Ultrasound generation and calibration

A custom-built 1-MHz F#-0.6 transducer was used to generate therapeutic ultrasound pulses. The transducer has eight identical two-inch diameter PZT disks mounted in an elliptical concave plastic housing with 18-cm diameter in the long axis, 16-cm diameter in the short axis and a radius of curvature of 106 mm (Fig. 1a). In the center of the housing is a 7 × 4-cm rectangular hole for the insertion of imaging probes. The transducer was driven by electronic input signals generated by a programmed field-programmable gate array (FPGA) (Altera Cyclone II, San Jose, CA) and amplified by a custom-built class D amplifier.

The pressure waveform and beam profiles of the therapeutic ultrasound were obtained in degassed water under free-field conditions using a custom-built fiber optic hydrophone with an active element of 100 μm diameter (Parsons et al. 2006b). Ultrasound pulses of 10-cycle duration at 1-MHz center frequency were used in all treatments. The peak negative (P−) and peak positive (P+) pressures were 21 and 59 MPa, respectively (Fig. 1b). The −6-dB beamwidths were estimated on both P− and P+ pressure profiles at P−/P+ pressure of 18/48 MPa. The −6-dB beamwidths measured 1.2 mm along the long lateral axis, 1.3 mm along the short lateral axis and 6.9 mm along the axial direction on the P− pressure profile. For the P+ profile, the −6-dB beamwidths measured 1.0 mm along the long lateral axis, 1.2 mm along the short lateral axis and 4.8 mm along the axial direction. The beam profiles at the experimental pressure level could not be measured because of the interference from the bubble cloud at the fiber tip. In the experimental setting, the acoustic intensity could be attenuated during the propagation path in the tissues. Given the 0.5 dB/cm/MHz attenuation in the liver (Parker et al. 1988) and a 1-cm mean propagation path, the P− pressure was likely 20 MPa. The P+ pressure was likely decayed more significantly to <56 MPa as a result of nonlinear attenuation.

Ultrasound treatment parameters

The treatments were performed using various time intervals (Δt) between successive pulses, with fixed numbers of pulses at 500 pulses for the RBC phantoms and 1000 pulses for the *ex vivo* tissues. The intervals, Δt, varied from 2, 10, 20, 50 and 100, to 200 ms in different treatments, because our previous study showed that the cavitation nuclei can persist up to several tens of ms after a histotripsy pulse (Xu et al. 2007b). These intervals were equal to or longer than those commonly used in the histotripsy treatments such that minimal thermal effects would occur in this study. Sixty-five treatments were performed on the RBC phantoms, resulting in a sample size of 10–12 for each Δt. Twenty-six *ex vivo* treatments were performed on the livers, resulting in a sample size of 4–5 for each.

Ultrasound treatment and monitoring

Before the treatment, the focus of the transducer was aligned with the RBC layer in the phantom using the following approach. A bubble cloud was first generated in the water using brief excitation of the transducer. The location of the bubble cloud was indicated using two 1-mm-wide 5-mW laser beams (Calpac Lasers, Steamboat Springs, CO), one along and the other perpendicular to the ultrasound beam, crossed at the middle of the bubble cloud. The phantom was then placed in the tank such that the RBC layer was aligned with the laser beams and thus to the ultrasound beam and along the long axis of the transducer (Fig. 2). For

the *ex vivo* treatments, the tissue samples were placed where the block of tissue phantom was.

During the treatment, the cavitation bubble clouds and the lesions were imaged with a 12-bit, 1280 × 960-pixel, high-speed camera (Phantom 210, Vision Research, Wayne, NJ). Backlighting was provided using a 300-W continuous white light lamp. This lighting allowed for a short exposure of 2 μs for each frame. The frame size was adjusted to be 16 × 12 mm using a Tominon macrobellows lens (Kyocera Optics, Nagano, Japan) attached to the camera. This image size ensured imaging of the overall bubble cloud and the entire lesion.

The imaging was performed after each pulse throughout the entire treatment. The bubbles were imaged 10 μs after the pulse because the spatial extent of the bubble cloud at this time corresponds well with that of the lesion (Maxwell et al. 2010b). The lesion image was taken at midperiod after the pulse when the cavitation bubbles disappeared on the optical images. This timing allowed for imaging of the lesions without interference from the bubbles for all Δts used in this study. Because the lesions may take several milliseconds and up to 1 s to become fully developed, another lesion image was taken approximately 5 s after the entire treatment to ensure that the maximum extent of the damage was imaged.

Cavitation pattern analysis

The cavitation bubbles appeared as dark shadows on the backlit images (*e.g.*, Fig. 3a), which can be easily distinguished from the background by the brightness. To detect the cavitation bubbles on the images, a pixel brightness threshold was set at *5* standard deviations below the average pixel brightness in a 2 × 2-mm region in the intact background area (light gray area on the images). The pixels with intensities lower than this threshold were considered in the areas of the cavitation bubbles. Using this threshold, the grayscale image was converted to a binary bubble image where 1 (white) represented the presence of bubbles and 0 (black) represented the absence of bubbles (Fig. 3b).

The effects of varying intervals between successive pulses on the cavitation patterns were studied by measuring: (1) the similarity, *i.e.*, cross correlation coefficient, between cavitation patterns in successive pulses; and (2) the integrated bubble area as the pulse number accumulated. The former assessed the level of the persistent cavitation memory. The latter indicated how fast the target volume can be completely “exposed” to or treated with the bubbles. The cross-correlation coefficient between cavitation patterns was calculated using the following equation:

$$\text{Cross correlation coefficient} = \frac{\sum_i X_k(i) X_{k+1}(i)}{\sqrt{\sum_i X_k(i)^2}\sqrt{\sum_i X_{k+1}(i)^2}}, \quad (1)$$

where $X_k(i)$ and $X_{k+1}(i)$ are the binary bubble images in the k-th and (k+1)-th pulses and i is the pixel index on the images. This coefficient was computed for each pair of successive pulses through the entire treatment, *i.e.*, $1 \leq k < 500$. To measure the integrated bubble area, an overlay of the bubble images was first formed for the k-th pulse by overlaying the binary bubble images from the first to the k-th pulse. The overlay image was also expressed in a binary format, where 1 indicated the presence of bubbles and 0 indicated the absence of bubbles in any pulse between the first and the k-th pulses. The integrated bubble area was computed by summing the areas with the presence of the bubbles on the overlay of the bubble images. The overlay outlined a region that could potentially be damaged in the treatments. The increasing trend of the integrated bubble area as the pulse number accumulated may predict the lesion-developing trend.

Lesion analysis

The damaged areas were significantly brighter than the intact areas (*e.g.*, Fig. 3c), and could be detected using a similar threshold approach. A pixel brightness threshold was set at 5 standard deviations above the average pixel brightness in a 2 × 2-mm region in the intact background area. Pixels with brightness higher than this threshold were considered "damaged." Using this threshold, the grayscale images were converted to binary lesion images where 1 (white) represented "damaged area" and 0 (black) represented "intact area" (Fig. 3d).

To study the lesion development process, the following analysis procedures were performed. First, the treatment zone was selected on the posttreatment lesion image by outlining a region that encompassed the maximal extent of the lesion, and then shaped like the overlay bubble image obtained in the previous section (cavitation pattern analysis). Next, the damaged area was calculated for each lesion image captured during the treatment by integrating the areas identified as "damaged" in the treatment zone. The damaged area was further normalized to the area of the treatment zone, resulting in the normalized damaged area. This normalized damaged area was compared for treatments using different time intervals between pulses.

Histologic examination

Histologic examination was conducted for the lesions produced in *ex vivo* tissues. After the treatments, the tissues were fixed in formalin and prepared for hematoxylin and eosin (H&E) staining. The lesions were sectioned longitudinally along the ultrasound beam. Multiple 4-μm thick H&E sections were made through the lesions with a 1-mm step size. The sections with the maximum spatial extent of damage both laterally and axially were examined through visual inspection with bright field microscopy. The homogeneity/heterogeneity, size, shape and boundary of the lesions were studied.

RESULTS

Cavitation patterns

Representative cavitation patterns induced during the treatments with decreasing time intervals between successive pulses are shown in Figure 4. The locations of the cavitation bubbles in response to each pulse were highly dependent on the time interval. When Δt was ≥100 ms, the cavitation bubbles were induced at distinctly different locations in response to each pulse. As Δt was decreased to <100 ms, many bubbles appeared at the same locations in each pulse. This repeated pattern was most prominent at the beginning of the treatment and became less significant as the pulse number increased.

The spatial extent of the bubble cloud was also affected by Δt. The bubble cloud appeared in a more confined area when Δt was ≥100 ms, and expanded as Δt decreased from 100 to 10 ms. As Δt further decreased to 2 ms, the bubble cloud was as large as that produced with Δt ranging between 100 and 10 ms at the beginning of the treatment, but appeared in a much smaller area around the center of the focus as the pulse number increased.

The cross-correlation coefficients between the cavitation patterns produced in successive pulses with varying Δts are plotted in Figure 5. The cross-correlation coefficient decreased exponentially with increasing Δts. This exponential decrease was particularly significant at the beginning of the treatment (*i.e.*, within 100 pulses). For example, the correlation coefficient at the 10^{th} pulses during the treatments with varying Δts decreased from 0.5 ± 0.1 to 0.1 ± 0.1 as Δt increased from 2 to 200 ms. These data were well fitted by an exponential curve ($r^2 = 0.96$, Fig. 5a). The exponential decay in the correlation coefficient

became less significant as the treatment continued because the correlation coefficient might change with increasing numbers of pulses (Fig. 5b–f). At the longest Δt (*i.e.*, 200 ms), the cross-correlation coefficient remained low at 0.1 ± 0.1 throughout the entire treatment. When Δt decreased to ≤20 ms, the correlation coefficient decreased from ~0.5 to ~0.1 as the pulse number increased from 0 to 500.

The overlay of the bubble images during the treatments with decreasing Δts are shown in Figure 6. When Δt was long, the bubbles occurred at random locations in each pulse. Therefore, the focal volume was fully exposed to the cavitation bubbles within a small number of pulses. When Δt was decreased, the focal volume was not fully exposed to the cavitation bubbles until a larger number of pulses was delivered. For instance, the focal volume was fully exposed to the bubbles within 100 pulses at Δt = 200 ms (Fig. 6a); however, it was not fully exposed until 500 pulses were delivered when Δt was decreased to 50 ms (Fig. 6c). When Δt was further decreased, some regions in the focal volume were never exposed to the cavitation bubbles during the entire treatment (Fig. 6e, f).

The integrated bubble areas during the treatments with varying Δts are shown in Figure 7. When Δt was ≥100 ms, the integrated bubble area rapidly increased with each additional pulse at the beginning of the treatment and reached a plateau at 100 pulses (Fig. 7a, b). This trend indicated that the target volume was fully exposed to the cavitation bubbles within a small number of pulses. As Δt was decreased from 100 to 10 ms, the increase in the integrated bubble areas slowed down, and a plateau was never observed within 500 pulses (Fig. 7c, e). When Δt was decreased to 2 ms, a plateau in the integrated bubble area was observed again (Fig. 7f). This plateau occurred for a different reason: the spatial extent of the bubble cloud decreased as the pulse number increased, thus limiting the growth of the overall bubble coverage area. This behavior is evidenced in Figure 4f as well where the spatial extent of the bubble cloud is limited in later pulses.

Lesion development process

Representative lesion images during the treatment illustrate the lesion development process with decreasing Δts (Fig. 8). In all treatments, damaged areas were detected after each pulse. The damaged area increased with increasing pulse numbers. The lesion developed more rapidly with each pulse for longer Δts. Furthermore, the lesion appeared to be homogeneously treated and possessed a smooth and well-defined boundary with no or very few residual intact areas in the treatment zone. As Δt was decreased, the lesions presented a ragged boundary with many residual intact areas.

The normalized damaged areas during the treatments with different Δts are shown in Figure 9a. The normalized damaged area increased more rapidly with each pulse when Δt was ≥100 ms. This increase slowed down as Δt decreased from 100 to 10 ms. The slowest increase was found at the shortest Δt, *i.e.*, 2 ms. After the treatments, complete fractionation of the treatment zone (*i.e.*, 100% damage) was achieved only when Δt was ≥50 ms. The normalized damaged area decreased when Δt was decreased. At Δt = 2 ms, only 50% of the treatment zone was damaged after the treatment. To compare the treatment efficiency for different Δts, the number of pulses required to achieve 25% damage was calculated (Fig. 9b). As Δt increased from 2 to 200 ms, the number of pulses required for 25% damage decreased from 199 ± 50 to 17 ± 9 pulses, approximately a 12-fold difference. This indicated that the treatment efficiency (defined as damage per pulse) was significantly higher for long Δts.

Ex vivo study

The *ex vivo* treatment results confirmed that the lesion morphology was highly dependent on the time intervals between pulses. With 1000 pulses applied, when Δt was ≥100 ms (Fig. 10a, b), the lesions appeared to be homogeneously and completely disrupted, with no or very few recognizable tissue structures in the treatment zone. The lesions also presented well-defined boundaries with sharp transition between the disrupted region and the surrounding structurally intact tissues. As Δt decreased from 50 to 20 ms (Fig. 10c, d), the lesions appeared to have a larger spatial extent; however, islands of incompletely disrupted tissue were present in the midst of the mostly treated zone. The tissue and cells within these islands appeared structurally intact when examined at higher magnification. Awider transition zone of scattered damaged spots was observed at the lesion boundaries. As Δt further decreased to below 20 ms (Fig. 10e, f), a significant amount of structurally intact tissue remained in the treatment zone. These results demonstrated that when the exposure was held small, complete tissue disruption was more likely achieved when Δt was increased.

DISCUSSION

We hypothesized that the cavitation memory may be removed by applying the subsequent pulse after a sufficiently long time interval after the previous pulse and that the removal of the memory may lead to complete and homogeneous tissue fractionation with fewer pulses. These hypotheses were supported by the results. At short time intervals between pulses, the highly correlated cavitation patterns indicated the presence of the cavitation memory. When the time interval between pulses was increased, the memory disappeared. As a result, the cavitation bubbles occurred in random locations in response to each pulse. The random patterns allowed the target volume to be fully exposed to cavitation within a significantly smaller number of pulses, leading to complete and homogeneous tissue fractionation with dramatically fewer pulses.

Despite the benefits of treatments with increased time interval between pulses, the total treatment time can be long if a large volume of tissue is treated by one single focal spot at a time. Because histotripsy pulses are only a few microseconds long, we propose using a 2-D phased array to steer the focus electronically to other locations within the treatment volume during the time between pulses (~100 ms). As such, the entire volume can be completely fractionated using the same time that is needed to fractionate a single focal spot. In this way, the treatment time to ablate a large tissue volume may be significantly reduced by increasing the duty cycle of the phased-array transducer.

To remove the cavitation memory, this study used a passive approach by increasing the time interval between pulses. In addition to this passive approach, active approaches can be used. For example, we have previously demonstrated that the persistent bubbles in the periphery of the focus can be actively removed by a nuclei preconditioning pulse delivered before each therapy pulse (Wang et al. 2010, 2011). A similar pulsing sequence may be developed to remove the persistent nuclei in the treatment volume. This pulsing sequence, if successfully developed, uses a special pulse to remove the cavitation memory immediately after each pulse. As soon as the cavitation memory is removed, the next therapy pulse can be delivered. Therefore, the time interval between successive pulses for the memory effect to disappear may be substantially reduced.

Although the presence of the cavitation memory caused highly correlated cavitation patterns at the beginning of the treatment, this correlation gradually decreased as the treatment continued. This decreasing correlation likely occurred because the progressive fractionation of the treatment volume, which eventually turned the treatment tissue volume to liquefied homogenate, provided increased mobility for the persistent cavitation nuclei. The similarity

between cavitation patterns was therefore decreased. Because this change only occurred in the later stage of the treatment, the overall treatment efficiency remained low compared with that of the treatments with uncorrelated cavitation patterns during the entire treatment.

The decreasing trend in the correlation coefficient of the cavitation patterns with increasing Δts indicated that the memory effects decayed exponentially with time and disappeared in several tens to hundreds of ms. The decay trend and period corresponded well with those of the residual bubbles that persisted in the treatment volume after a histotripsy pulse (Xu et al. 2007b). The decay period also corresponded well with the dissolution time of micron-sized gas bubbles (Epstein and Plesset 1950; Chen et al. 2002; Ferrara et al. 2007). These suggested that the persistent gas bubbles are an important source causing the memory effect. It is not excluded that the fragments of fractionated tissues or tissue phantoms may also serve as potential cavitation nuclei that contribute to the memory effect.

The normalized damaged area measured during the treatments (Fig. 9a) may be slightly underestimated because of the limitation in the temporal response of the RBC phantoms. The damage was imaged 1–100 ms after each pulse; however, it may take several milliseconds for the lesions to become fully developed. This latency could have caused different amounts of underestimation for various Δts. To evaluate the amount of underestimation, the damaged areas measured at the last pulse of the treatments and 5 s after the treatments (two rightmost columns in Fig. 8) were compared. The differences between the two measurements were found to be 0.1–1.2 mm^2, with the maximum occurring for Δt = 2 ms. In the worst case, this difference would cause an underestimation of the normalized damaged area by 7%. This amount is small compared with the difference caused by different experimental conditions, and thus should have minimal influence on the trends observed in Figure 9a.

In the present work, histotripsy is applied inside the tissue phantoms or tissues where the nuclei movement is restricted and bubble expansion is constrained. The same experiments have been performed at a fluid-stone interface set up as described in our previous paper (Duryea et al. 2011). Preliminary results showed that the shape of the overall bubble cloud was similar from pulse to pulse; however, the individual bubbles did not repeatedly occur in the same locations as observed in the tissue phantoms. Although the pulse parameters used in this test are histotripsy rather than lithotripsy parameters, this observation suggests that the repeated cavitation pattern may be less significant in a fluid environment (*e.g.*, in lithotripsy) and more of a concern in a tissue environment (*e.g.*, in histotripsy).

An interesting evolutionary trend of the bubble cloud induced at the shortest time interval between pulses (*i.e.*, 2 ms), or the highest pulsing rate, was observed. The spatial extent of the bubble cloud decreased to a smaller area around the focal center as the pulse number increased. This phenomenon may have resulted from significant decrease in the available cavitation nuclei in the treatment volume. The available cavitation nuclei in the target volume could have been quickly depleted after repetitive pulsing at a high pulsing rate (Borkent et al. 2007). In addition, the short interval between pulses could have impeded the replenishment of new cavitation nuclei from the surrounding area. The depletion of the available nuclei may have raised the cavitation threshold in the treatment volume, therefore restricting bubbles to a smaller area where the pressure amplitude remained above the new threshold. Further investigation is needed to elucidate the mechanisms behind this phenomenon.

CONCLUSIONS

This study demonstrated that cavitation memory may have distinct influence on the lesion development process in histotripsy. The cavitation memory effect resulted in highly correlated cavitation patterns, leading to slow development of lesions with each pulse. The removal of the memory effect caused cavitation bubbles to occur in new random locations in response to each pulse, resulting in complete and homogeneous tissue disruption with significantly fewer pulses, *i.e.*, more efficient treatments. Moreover, in real-time monitoring of lesion development, homogeneously disrupted lesions should result in tissue characterization metrics representative of the whole lesion instead of a misleading average of fully homogenized and nonhomogenized zones. This may be potentially important in image-guided cancer therapy.

Acknowledgments

This work is supported by the NIH (grants R01 CA134579 and R01 EB008998).

References

Arora M, Junge L, Ohl CD. Cavitation cluster dynamics in shock-wave lithotripsy: Part 1. Free field Ultrasound Med Biol. 2005; 31:827–839.

Borkent BM, Arora M, Ohl CD. Reproducible cavitation activity in water-particle suspensions. J Acoust Soc Am. 2007; 121:1406–1412. [PubMed: 17407877]

Chen WS, Matula TJ, Crum LA. The disappearance of ultrasound contrast bubbles: Observations of bubble dissolution and cavitation nucleation. Ultrasound Med Biol. 2002; 28:793–803. [PubMed: 12113792]

Delius M, Brendel W. A model of extracorporeal shock wave action: Tandem action of shock waves. Ultrasound Med Biol. 1988; 14:515–518. [PubMed: 3227574]

Delius M, Jordan M, Eizenhoefer H, Marlinghaus E, Heine G, Liebich HG, Brendel W. Biological effects of shock waves: Kidney haemorrhage by shock waves in dogs—administration rate dependence. Ultrasound Med Biol. 1988; 14:689–694. [PubMed: 3212839]

Duryea AP, Maxwell AD, Roberts WW, Xu Z, Hall TL, Cain CA. In vitro comminution of model renal calculi using histotripsy. IEEE Trans Ultrason Ferroelectr Freq Control. 2011; 58:971–980. [PubMed: 21622053]

Epstein PS, Plesset MS. On the stability of gas bubbles in liquid-gas solutions. J Chem Phys. 1950; 18:1505–1509.

Ferrara K, Pollard R, Borden M. Ultrasound microbubble contrast agents: Fundamentals and application to gene and drug delivery. Annu Rev Biomed Eng. 2007; 9:415–447. [PubMed: 17651012]

Flynn HG, Church CC. A mechanism for the generation of cavitation maxima by pulsed ultrasound. J Acoust Soc Am. 1984; 76:505–512. [PubMed: 6481000]

Fowlkes JB, Crum LA. Cavitation threshold measurements for microsecond length pulses of ultrasound. J Acoust Soc Am. 1988; 83:2190–2201. [PubMed: 3411016]

Fox FE, Herzfeld KF. Gas bubbles with organic skin as cavitation nuclei. J Acoust Soc Am. 1954; 26:984–989.

Harvey EN, Barnes DK, McElroy WD, Whiteley AH, Pease DC, Cooper KW. Bubble formation in animals. I. Physical factors. J Cell Comp Physiol. 1944a; 24:1–22.

Harvey EN, Barnes DK, McElroy WD, Whiteley AH, Pease DC, Cooper KW. Bubble formation in animals. II. Gas nuclei and their distribution in blood and tissues. J Cell CompPhysiol. 1944b; 24:23–34.

Henglein A, Gutierrez M. Chemical reactions by pulsed ultrasound: Memory effects in the formation of NO3- and NO2- in aerated water. Int J Radiat Biol Relat Stud Phys Chem Med. 1986; 50:527–533. [PubMed: 3488974]

Huber P, Debus J, Jochle K, Simiantonakis I, Jenne J, Rastert R, Spoo J, Lorenz WJ, Wannenmacher M. Control of cavitation activity by different shockwave pulsing regimes. Phys Med Biol. 1999; 44:1427–1437. [PubMed: 10498515]

Huber P, Jochle K, Debus J. Influence of shock wave pressure amplitude and pulse repetition frequency on the lifespan, size and number of transient cavities in the field of an electromagnetic lithotripter. Phys Med Biol. 1998; 43:3113–3128. [PubMed: 9814538]

Kieran K, Hall TL, Parsons JE, Wolf JS Jr, Fowlkes JB, Cain CA, Roberts WW. Refining histotripsy: Defining the parameter space for the creation of nonthermal lesions with high intensity, pulsed focused ultrasound of the in vitro kidney. J Urol. 2007; 178:672–676. [PubMed: 17574617]

Kim Y, Gelehrter SK, Fifer CG, Lu JC, Owens GE, Berman DR, Williams J, Wilkinson JE, Ives KA, Xu Z. Non-invasive pulsed cavitational ultrasound for fetal tissue ablation: Feasibility study in a fetal sheep model. Ultrasound Obstet Gynecol. 2011; 37:450–457. [PubMed: 21433165]

Leighton, TG. The acoustic bubble. Waltham, MA: Academic Press; 1997.

Lizzi FL, Astor M, Liu T, Deng C, Coleman DJ, Silverman RH. Ultrasonic spectrum analysis for tissue assays and therapy evaluation. Intl J Imaging Sys Tech. 1997; 8:3–10.

Loske AM, Prieto FE, Fernandez F, van Cauwelaert J. Tandem shock wave cavitation enhancement for extracorporeal lithotripsy. Phys Med Biol. 2002; 47:3945–3957. [PubMed: 12476975]

Madbouly K, El-Tiraifi AM, Seida M, El-Faqih SR, Atassi R, Talic RF. Slow versus fast shock wave lithotripsy rate for urolithiasis: A prospective randomized study. J Urol. 2005; 173:127–130. [PubMed: 15592053]

Maxwell AD, Owens G, Gurm HS, Ives K, Myers DD Jr, Xu Z. Noninvasive treatment of deep venous thrombosis using pulsed ultrasound cavitation therapy (histotripsy) in a porcine model. J Vasc Interv Radiol. 2010a; 22:369–377. [PubMed: 21194969]

Maxwell AD, Wang T-Y, Yuan L, Duryea AP, Xu Z, Cain CA. A tissue phantom for evaluation of mechanical damage caused by cavitation. Ultrasound Med Biol. 2010b; 36:2132–2143. [PubMed: 21030142]

Maxwell AD, Wang TY, Cain CA, Fowlkes JB, Sapozhnikov OA, Bailey MR, Xu Z. Cavitation clouds created by shock scattering from bubbles during histotripsy. J Acoust Soc Am. 2011; 130:1888–1898. [PubMed: 21973343]

Owens GE, Miller RM, Ensing G, Ives K, Gordon D, Ludomirsky A, Xu Z. Therapeutic ultrasound to noninvasively create intracardiac communications in an intact animal model. Catheter Cardiovasc Interv. 2010; 77:580–588. [PubMed: 20853366]

Parker KJ, Asztely MS, Lerner RM, Schenk EA, Waag RC. In-vivo measurements of ultrasound attenuation in normal or diseased liver. Ultrasound Med Biol. 1988; 14:127–136. [PubMed: 3279691]

Parsons JE, Cain CA, Abrams GD, Fowlkes JB. Pulsed cavitational ultrasound therapy for controlled tissue homogenization. Ultrasound Med Biol. 2006a; 32:115–129. [PubMed: 16364803]

Parsons JE, Cain CA, Fowlkes JB. Cost-effective assembly of a basic fiber-optic hydrophone for measurement of high-amplitude therapeutic ultrasound fields. J Acoust Soc Am. 2006b; 119:1432–1440. [PubMed: 16583887]

Paterson RF, Lifshitz DA, Lingeman JE, Evan AP, Connors BA, Fineberg NS, Williams JC Jr, McAteer JA. Stone fragmentation during shock wave lithotripsy is improved by slowing the shock wave rate: Studies with a new animal model. J Urol. 2002; 168:2211–2215. [PubMed: 12394761]

Pishchalnikov YA, McAteer JA, Williams JC Jr, Pishchalnikova IV, Vonderhaar RJ. Why stones break better at slow shockwave rates than at fast rates: In vitro study with a research electrohydraulic lithotripter. J Endourol. 2006; 20:537–541. [PubMed: 16903810]

Roberts WW, Hall TL, Ives K, Wolf JS Jr, Fowlkes JB, Cain CA. Pulsed cavitational ultrasound: a noninvasive technology for controlled tissue ablation (histotripsy) in the rabbit kidney. J Urol. 2006; 175:734–738. [PubMed: 16407041]

Ryan PC, Jones BJ, Kay EW, Nowlan P, Kiely EA, Gaffney EF, Butler MR. Acuteand chronicbioeffects of single and multiple doses of piezoelectric shockwaves (EDAP LT.01). J Urol. 1991; 145:399–404. [PubMed: 1824866]

Sapozhnikov OA, Khokhlova VA, Bailey MR, Williams JC Jr, McAteer JA, Cleveland RO, Crum LA. Effect of overpressure and pulse repetition frequency on cavitation in shock wave lithotripsy. J Acoust Soc Am. 2002; 112:1183–1195. [PubMed: 12243163]

Styn NR, Wheat JC, Hall TL, Roberts WW. Histotripsy of VX-2 tumor implanted in a renal rabbit model. J Endourol. 2010; 24:1145–1150. [PubMed: 20575696]

Wang T-Y, Xu Z, Hall T, Fowlkes JB, Roberts WW, Cain CA. Active focal zone sharpening for high precision treatment using histotripsy. IEEE Trans Ultrason Ferroelect Freq Control. 2011:305–315.

Wang T-Y, Hall TL, Xu Z, Fowlkes JB, Cain CA. Local cavitation suppression using cavitation nuclei preconditioning for precise treatment in histotripsy. Proc IEEE Ultrason Symp. 2010:334–337.

Wang T-Y, Xu Z, Winterroth F, Hall TL, Fowlkes JB, Rothman ED, Roberts WW, Cain CA. Quantitative ultrasound backscatter for pulsed cavitational ultrasound therapy—histotripsy. IEEE Trans Ultrason Ferroelectr Freq Control. 2009; 56:995–1005. [PubMed: 19750596]

Weir MJ, Tariq N, Honey RJ. Shockwave frequency affects fragmentation in a kidney stone model. J Endourol. 2000; 14:547–550. [PubMed: 11030533]

Xi X, Zhong P. Improvement of stone fragmentation during shock-wave lithotripsy using a combined EH/PEAA shock-wave generator-in vitro experiments. Ultrasound Med Biol. 2000; 26:457–467. [PubMed: 10773377]

Xu Z, Fowlkes JB, Cain CA. A new strategy to enhance cavitational tissue erosion using a high-intensity, initiating sequence. IEEE Trans Ultrason Ferroelect Freq Control. 2006; 53:1412–1424.

Xu Z, Fowlkes JB, Rothman ED, Levin AM, Cain CA. Controlled ultrasound tissue erosion: The role of dynamic interaction between insonation and microbubble activity. J Acoust Soc Am. 2005; 117:424–435. [PubMed: 15704435]

Xu Z, Hall TL, Fowlkes JB, Cain CA. Effects of acoustic parameters on bubble cloud dynamics in ultrasound tissue erosion (histotripsy). J Acoust Soc Am. 2007a; 122:229–236. [PubMed: 17614482]

Xu Z, Hall TL, Fowlkes JB, Cain CA. Optical and acoustic monitoring of bubble cloud dynamics at a tissue-fluid interface in ultrasound tissue erosion. J Acoust Soc Am. 2007b; 121:2421–2430. [PubMed: 17471753]

Xu Z, Ludomirsky A, Eun LY, Hall TL, Tran BC, Fowlkes JB, Cain CA. Controlled ultrasound tissue erosion. IEEE Trans Ultrason Ferroelect Freq Control. 2004; 51:726–736.

Xu Z, Owens G, Gordon D, Cain C, Ludomirsky A. Noninvasive creation of an atrial septal defect by histotripsy in a canine model. Circulation. 2010; 121:742–749. [PubMed: 20124126]

Xu Z, Raghavan M, Hall TL, Mycek MA, Fowlkes JB, Cain CA. Evolution of bubble clouds induced by pulsed cavitational ultrasound therapy—histotripsy. IEEE Trans Ultrason Ferroelectr Freq Control. 2008; 55:1122–1132. [PubMed: 18519220]

Yavas O, Leiderer P, Park HK, Grigoropoulos CP, Poon CC, Tam AC. Enhanced acoustic cavitation following laser-induced bubble formation: Long-term memory effect. Phys Rev Lett. 1994; 72:2021–2024. [PubMed: 10055768]

Yilmaz E, Batislam E, Basar M, Tuglu D, Mert C, Basar H. Optimal frequency in extracorporeal shock wave lithotripsy: Prospective randomized study. Urology. 2005; 66:1160–1164. [PubMed: 16360432]

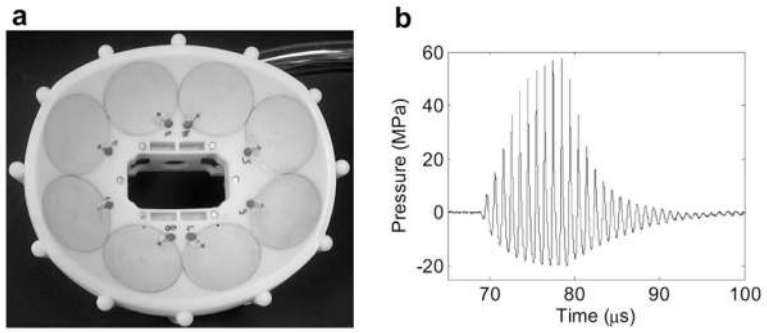

Fig. 1.
(a) A picture of the therapeutic transducer and (b) pressure waveform of the therapy pulse measured under free-field conditions in water.

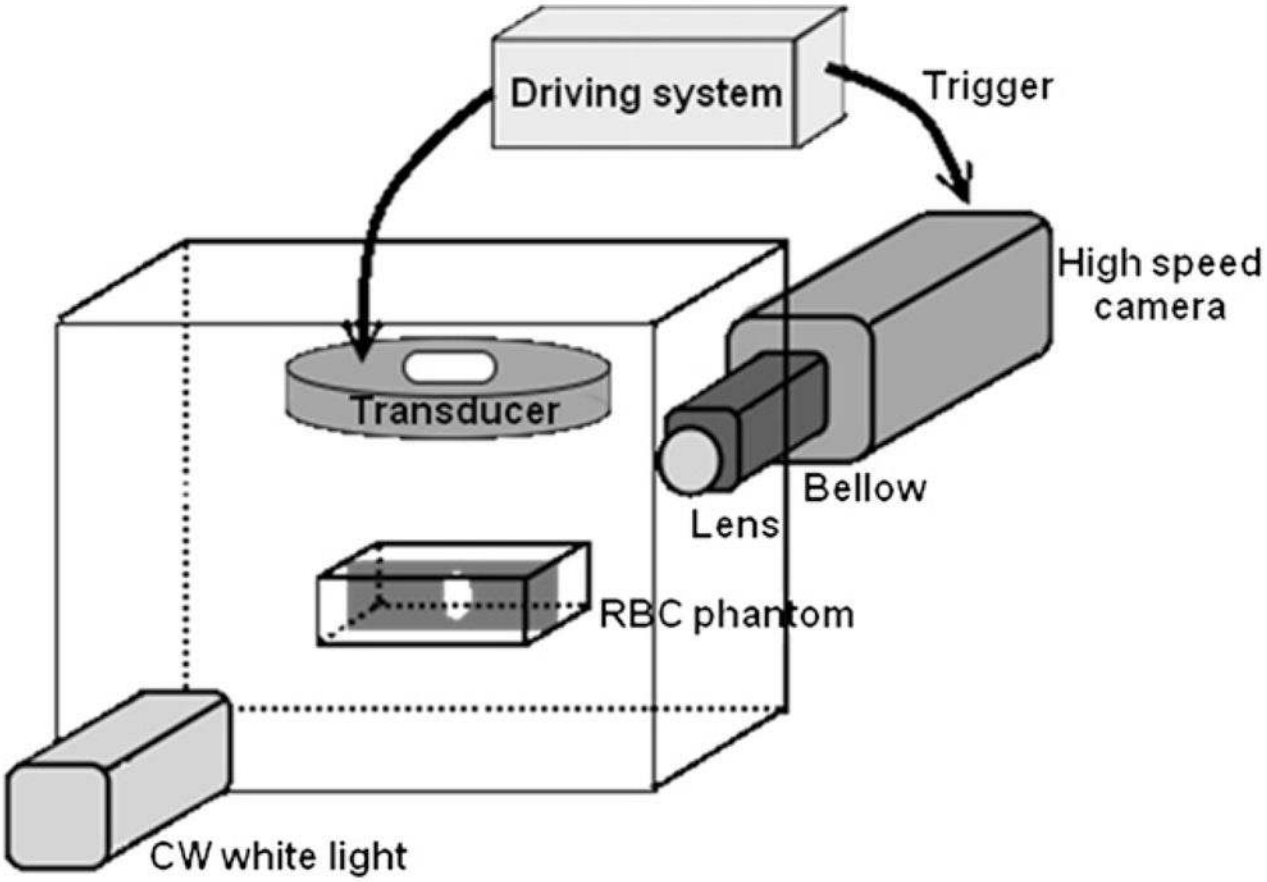

Fig. 2.

Experimental setup. The transducer and the RBC phantom are submerged in a tank filled with degassed water (30% of normal saturation determined by pO_2). The high-speed camera was mounted perpendicular to the ultrasound beam such that a projection of the bubble cloud and the lesions on the axial-lateral plane of the transducer were recorded.

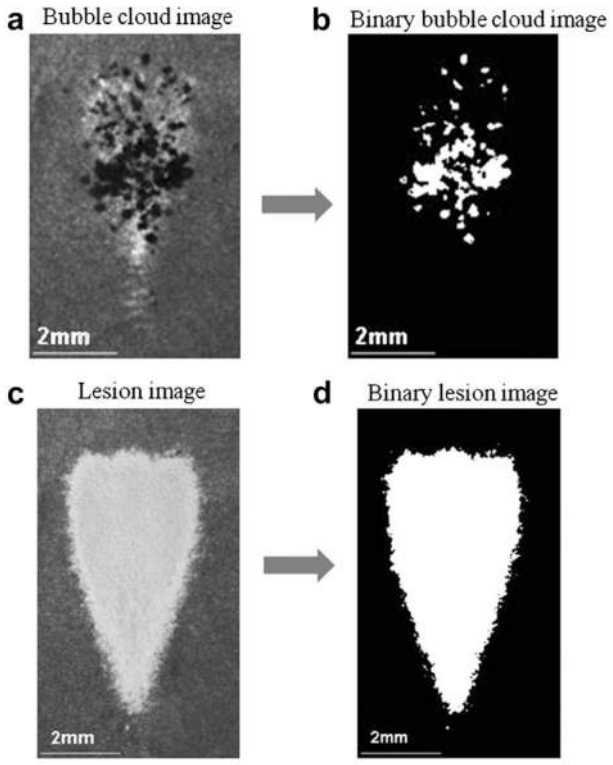

Fig. 3.

Examples of converting the grayscale images to binary images for the cavitation bubble clouds (panel (a)–(b)) and the lesions (panel (c)–(d)). Longitudinal sections of the bubble clouds and the lesions are shown. The ultrasound propagation direction is from top to bottom of the image.

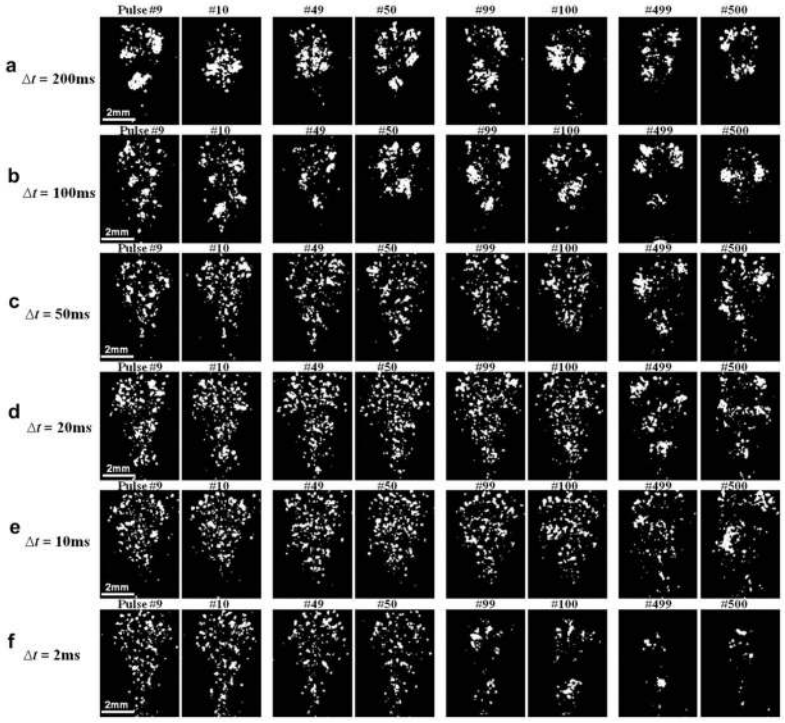

Fig. 4.

Cavitation patterns generated by successive pulses (pulses #9 and #10, #49 and #50, #99 and #100, #499 and #500) during the treatments when the time interval between pulses, Δt, decreased from (a) 200 to (f) 2 ms. The ultrasound propagation direction is from top to bottom of the image. The cavitation patterns in successive pulses appeared distinctly different in response to each pulse when Δt was long (*e.g.*, panel (a)), but they were relatively similar when Δt was decreased (*e.g.*, panel (f)).

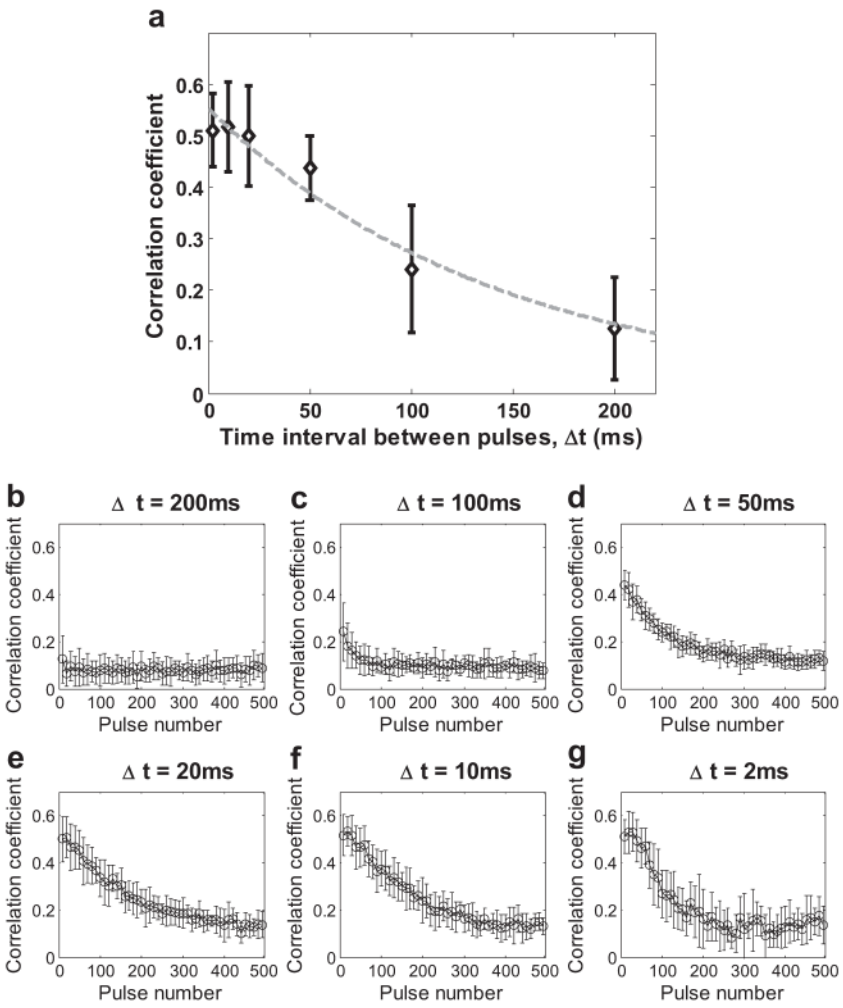

Fig. 5.

Cross-correlation coefficients of cavitation patterns induced in successive pulses for decreasing time intervals between pulses. The correlation coefficient decreased exponentially with increasing Δts at the beginning of the treatment (<100 pulses). As an example, the correlation coefficients at the 10^{th} pulse is shown in panel (a) (dashed line: $y = 0.55e^{-7.06t}$, $r^2 = 0.96$). The exponential decay in the correlation coefficient became less significant later as the pulse number increased because the correlation coefficient might change (panels (b)–(f)). Data are presented in mean ± standard deviation (n = 10–12 each).

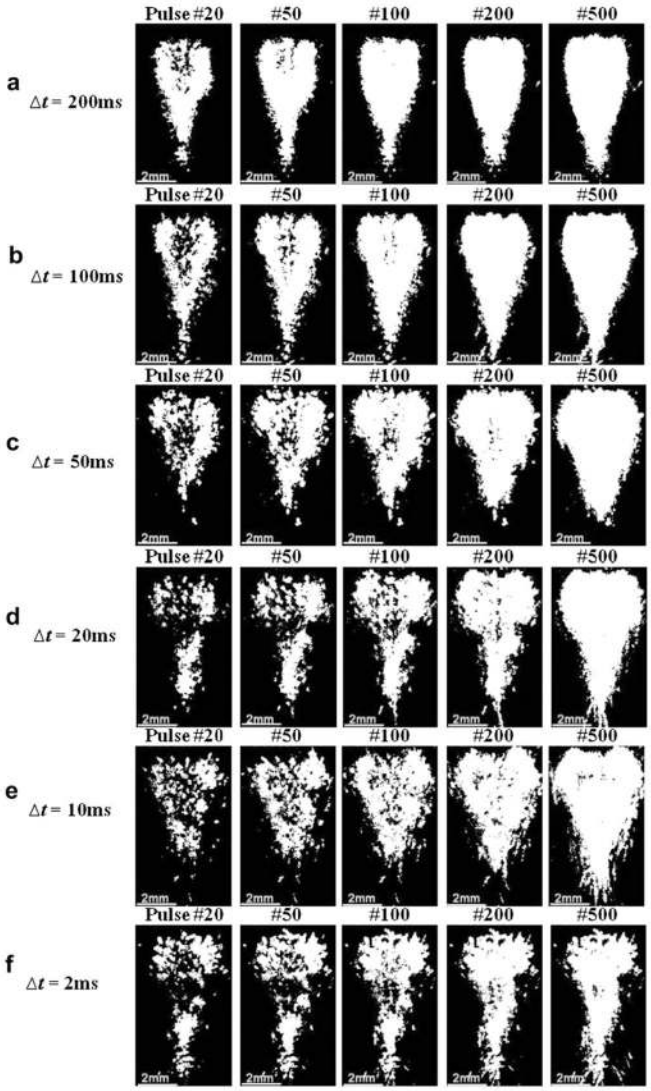

Fig. 6.

Overlay of the bubble images during the treatments when the time intervals between pulses decreased from (a) 200 to (f) 2 ms. The ultrasound propagation direction is from top to bottom of the image. When Δt was long, the focal volume was fully exposed to the cavitation bubbles within a small number of pulses (panel (a)). The number of pulses needed for the focal volume to be fully exposed to cavitation increased when Δt was decreased. When Δt was too short, full exposure could not be achieve within 500 pulses, and islands of untreated areas were present after the treatments (panels (e) and (f)).

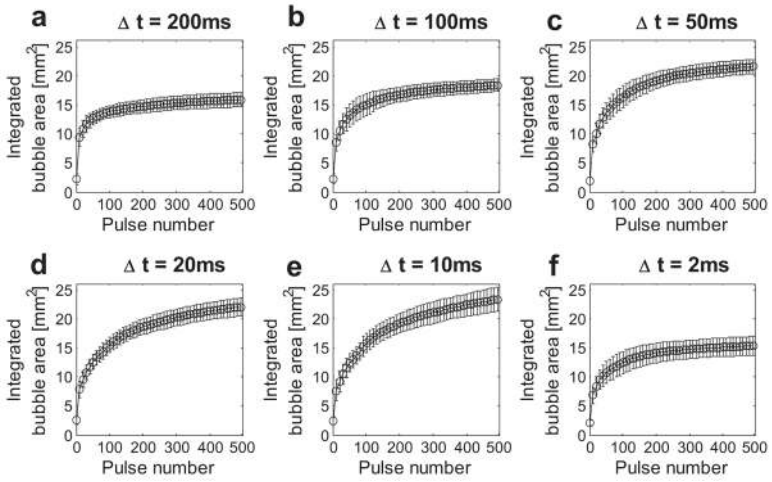

Fig. 7.

Integrated bubble areas with increasing pulse numbers when the time intervals between pulses decreased from (a) 200 to (f) 2 ms. The integrated bubble area increased rapidly and reached a plateau when Δt was long. When Δt was decreased, the increasing trend slowed down, and the plateau was not observed. When Δt was decreased to 2 ms, a plateau occurred again because the decreased spatial extent of the bubble cloud limited the growth of the integrated bubble area. Data are presented as mean ± standard deviation (n = 10 to 12).

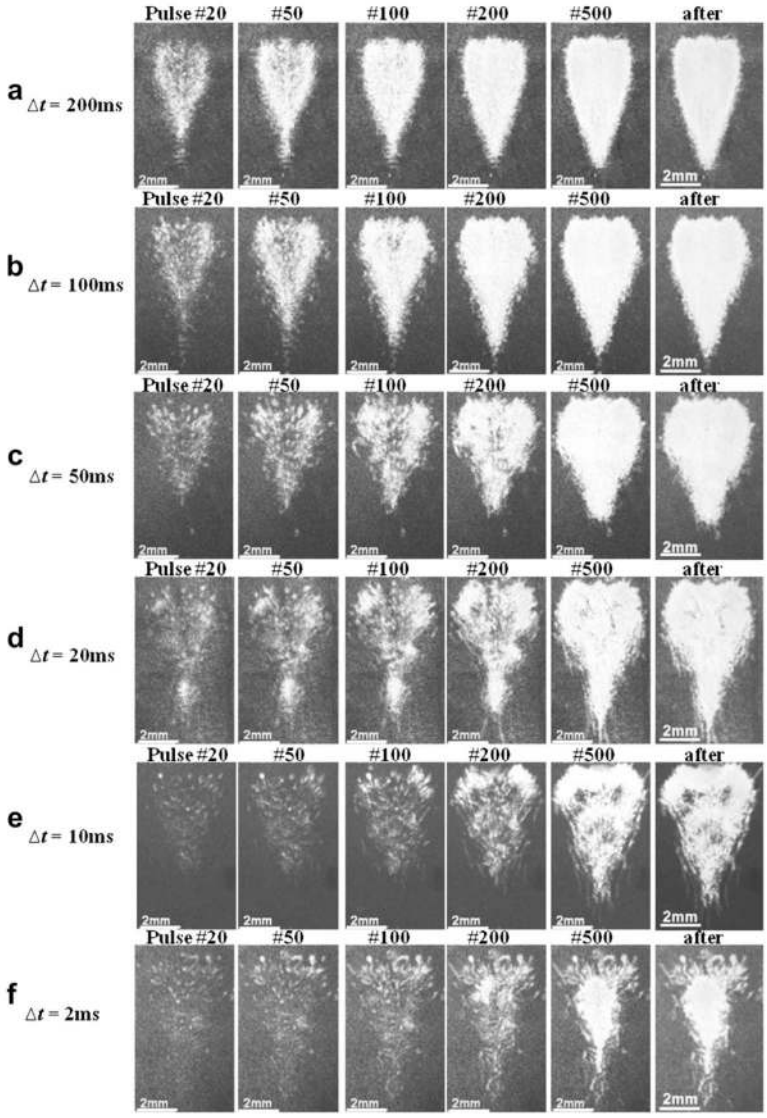

Fig. 8.

The lesion patterns observed during and after the treatments when the time intervals between pulses decreased from (a) 200 to (f) 2 ms. The ultrasound propagation direction is from top to bottom of the image. At long Δts, the damaged area rapidly expanded with each pulse; completely fractionated lesions were observed after the treatments. At short Δts, the damaged area developed slowly with each pulse; incompletely treated lesions with islands of untreated areas were observed after the treatments.

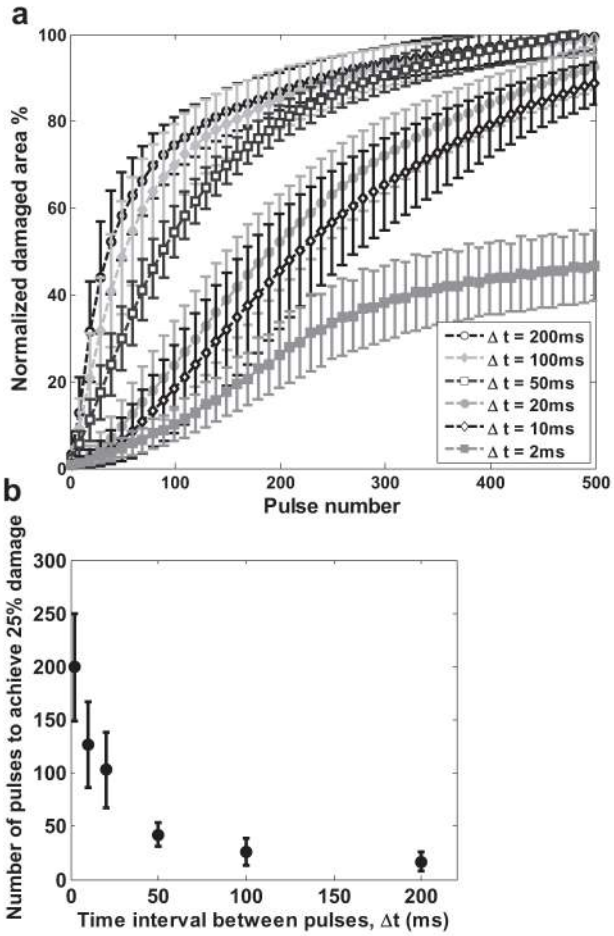

Fig. 9.

(a) Normalized damaged areas during the treatments with different time intervals between pulses, Δts. Lesions produced with longer Δts developed significantly faster with each pulse than those produced with shorter Δts. Complete disruption of the treatment zone was achieved only when Δt was ≥50 ms. (b) Number of pulses to achieve 25% damage for different Δts. The required number of pulses was reduced by approximately 12-fold as Δt increased from 2 to 200 ms. Data are presented as mean ± standard deviation (n = 10 to 12).

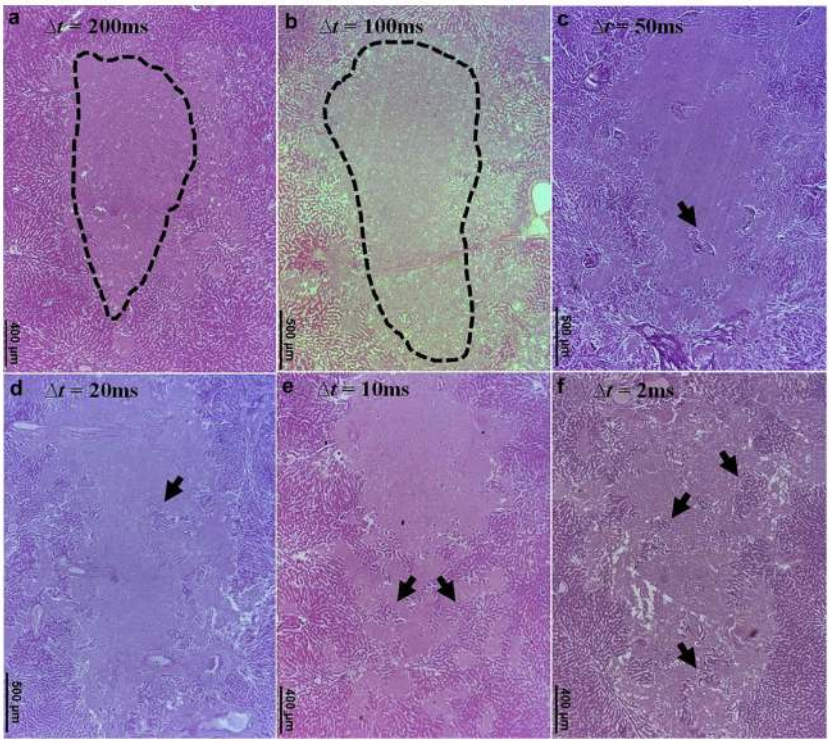

Fig. 10.

Lesions produced in *ex vivo* livers using 1000 pulses when the time intervals between pulses decreased from (a) 200 to (f) 2 ms. The ultrasound propagation direction is from top to bottom of the image. When Δt was ≥100 ms, completely homogenized lesions were observed (outlined by the dashed lines in panels (a) and (b)). As Δt decreased, isolated islands of structurally intact areas were observed in the treatment volume (*e.g.*, the areas indicated by the arrows in panels (c)–(f)). More islands of structurally intact areas appeared as Δt further decreased.